Available online at www.sciencedirect.com
ScienceDirect
Precision Engineering 31 (2007) 251–259
PRECISION ENGINEERING
www.elsevier.com/locate/precision

Monte Carlo evaluation of periodic error uncertainty

Tony L. Schmitz*, Hyo Soo Kim

Machine Tool Research Center, University of Florida, 237 MAE-B, Gainesville, FL 32611, United States

Received 9 August 2006; accepted 11 October 2006
Available online 12 December 2006

Abstract

This paper presents a single analytical expression for the displacement recorded using a polarization-coded, heterodyne interferometer in terms of the various uncertainty contributors, including periodic error and other phase nonlinearities, Abbe error, cosine error, deadpath error, environmental error, interferometer thermal effects, and wavelength stability. The displacement equation is based on the periodic error expression reported by Cosijns et al. Monte Carlo simulation is applied to determine the first and second order periodic error uncertainty. The Monte Carlo simulation is then extended to include the other uncertainty contributors included in the analytical displacement equation.

Keywords: Interferometry; Displacement; Uncertainty; Nonlinearity

1. Introduction

Periodic error, or nonlinearity, in displacement measuring interferometry is a well-known phenomenon. It has been shown by multiple authors that cyclical, or non-cumulative, errors are superimposed on the measurement signal due to non-ideal performance of the interferometer components and imperfect alignment of the laser source and optics [1–31]. Errors of both one (first order) and two (second order) cycles per displacement fringe have been observed.

Evaluation of the overall uncertainty in displacement measuring interferometry has traditionally followed the "error budget" technique where the individual error contributors are individually determined (either through statistical or other analyses) and then combined, often using a root sum squares, or RSS, approach [32,33]. These contributors, which may include Abbe error, cosine error, deadpath error, environmental error, air (or other medium) turbulence, beam shear, thermal effects, electronics linearity, laser wavelength stability, and periodic error, are tabulated so that primary offenders may be identified and compensated or corrected [34]. This is an effective and time-proven method. However, to the authors' knowledge, a single analytical expression that describes displacement, l, in terms of the multiple inputs that determine its value has not been presented. This precludes the use of a Taylor series expansion of the measurand [35,36] and/or Monte Carlo simulation to evaluate the combined standard uncertainty, $u_c(l)$, for the measurement result.

In this work we augment the analytical periodic error expression presented by Cosijns et al. [37] with terms that describe the other error sources listed previously to arrive at a single expression for displacement. We then propagate uncertainty contributors through this equation to determine the combined standard uncertainty, u_c, in the measurement result. The paper is organized as follows: first, the Cosijns et al. expression is presented (Section 2) and example error distributions are shown for various periodic error conditions; second, a single pass, heterodyne interferometer setup, designed to isolate periodic error as the primary uncertainty source, is detailed (Section 3) and measurement results are provided; finally, the additional uncertainty contributors are appended to the displacement equation and the uncertainty evaluation is demonstrated using Monte Carlo simulation (Section 4).

2. Periodic error formulation

In this paper we focus on Michelson-type interferometers with a two frequency laser source (i.e., heterodyne interferometry). In these systems, imperfect separation of the two light frequencies into the measurement (moving) and reference (fixed) paths produce the first and second order periodic errors. The two frequencies are typically carried on collinear, mutually

* Corresponding author. Tel.: +1 352 392 8909; fax: +1 352 392 1071.
E-mail address: tschmitz@ufl.edu (T.L. Schmitz).

0141-6359/$ – see front matter © 2006 Elsevier Inc. All rights reserved.
doi:10.1016/j.precisioneng.2006.10.001

orthogonal, linear polarizations in a method referred to as polarization coding. Unwanted leakage of the reference frequency into the measurement path, and vice versa, may occur due to a number of influences, including non-orthogonality between the ideally linear beam polarizations, elliptical polarization of the individual beams, non-ideal performance of the optical components, and/or mechanical misalignment between the interferometer elements (laser, polarizing optics, and targets). In a perfect system, a single frequency would travel to a fixed target, while a second, single frequency traveled to a moving target. Interference of the combined signals would yield a perfectly sinusoidal trace with phase that varied, relative to a reference phase signal, in response to motion of the moving target. However, the inherent frequency leakage in actual implementations produces an interference signal which is not purely sinusoidal and leads to periodic error in the measured displacement.

The Cosijns et al. analysis propagates: ellipticity of the two (nominally linear) polarizations; non-orthogonality between the two polarizations; rotation of the polarization axes relative to the polarizing beam splitter (which ideally separates the collinear frequencies into the measurement and reference paths); transmission coefficient variations for the polarizing beam splitter; rotation of the measurement polarizer, which causes interference of the measurement and reference beams, relative to its nominal 45° orientation (for vertical and horizontal source polarizations), through the interference equations to arrive an expression for the periodic phase error, $\Delta\phi_{\mathrm{pe}}$. See Eq. (1), where θ is the deviation of the polarizer angle from 45° and the variables A–F are defined in Eqs. (2)–(7).

$$\Delta\phi_{\mathrm{pe}} = -\tan^{-1}\left(\frac{A + B\,\sin(2\theta) + C\,\cos(2\theta)}{D + E\,\sin(2\theta) + F\,\cos(2\theta)}\right) \tag{1}$$

$$A = \left(-(\xi^2\,\sin(\beta)^2 + \chi^2\,\cos(\beta)^2)\cos\left(\frac{d\varepsilon_1}{2}\right)\sin\left(\frac{d\varepsilon_2}{2}\right) - (\xi^2\,\cos(\alpha)^2 + \chi^2\,\sin(\alpha)^2)\sin\left(\frac{d\varepsilon_1}{2}\right)\cos\left(\frac{d\varepsilon_2}{2}\right)\right)\cos(\Delta\phi)$$
$$+(\xi^2\,\cos(\alpha)\sin(\beta) + \chi^2\,\sin(\alpha)\cos(\beta))\cos\left(\frac{d\varepsilon_1}{2} + \frac{d\varepsilon_2}{2}\right)\sin(\Delta\phi) \tag{2}$$

$$B = \left(\xi^2\,\sin(\beta)^2 - \chi^2\,\cos(\beta)^2)\cos\left(\frac{d\varepsilon_1}{2}\right)\sin\left(\frac{d\varepsilon_2}{2}\right) + (\xi^2\,\cos(\alpha)^2 - \chi^2\,\sin(\alpha)^2)\sin\left(\frac{d\varepsilon_1}{2}\right)\cos\left(\frac{d\varepsilon_2}{2}\right)\right)(\cos(\Delta\phi)$$
$$+(-\xi^2\,\cos(\alpha)\sin(\beta) + \chi^2\,\sin(\alpha)\cos(\beta))\cos\left(\frac{d\varepsilon_1}{2} + \frac{d\varepsilon_2}{2}\right)\sin(\Delta\phi) \tag{3}$$

$$C = \xi\chi\left(\cos(\beta)\sin(\beta)\cos\left(\frac{d\varepsilon_1}{2}\right)\sin\left(\frac{d\varepsilon_2}{2}\right)(1 - \cos(2\Delta\phi)) + \sin(\alpha)\sin(\beta)\cos\left(\frac{d\varepsilon_1}{2}\right)\cos\left(\frac{d\varepsilon_2}{2}\right)\sin(2\Delta\phi)\right.$$
$$\left. - \cos(\alpha)\cos(\beta)\sin\left(\frac{d\varepsilon_1}{2}\right)\sin\left(\frac{d\varepsilon_2}{2}\right)\sin(2\Delta\phi) - \sin(\alpha)\cos(\alpha)\sin\left(\frac{d\varepsilon_1}{2}\right)\cos\left(\frac{d\varepsilon_2}{2}\right)(1 + \cos(2\Delta\phi))\right) \tag{4}$$

$$D = \left((\xi^2\,\sin(\beta)^2 + \chi^2\,\cos(\beta)^2)\cos\left(\frac{d\varepsilon_1}{2}\right)\sin\left(\frac{d\varepsilon_2}{2}\right) + (\xi^2\,\cos(\alpha)^2 + \chi^2\,\sin(\alpha)^2)\sin\left(\frac{d\varepsilon_1}{2}\right)\cos\left(\frac{d\varepsilon_2}{2}\right)\right)\sin(\Delta\phi)$$
$$+(-\xi^2\,\cos(\alpha)\sin(\beta) + \chi^2\,\sin(\alpha)\cos(\beta))\cos\left(\frac{d\varepsilon_1}{2} + \frac{d\varepsilon_2}{2}\right) + \cos(\Delta\phi) \tag{5}$$

$$E = \left((-\xi^2\,\sin(\beta)^2 + \chi^2\,\cos(\beta)^2)\cos\left(\frac{d\varepsilon_1}{2}\right)\sin\left(\frac{d\varepsilon_2}{2}\right) + (-\xi^2\,\cos(\alpha)^2 + \chi^2\,\sin(\alpha)^2)\sin\left(\frac{d\varepsilon_2}{2}\right)\cos\left(\frac{d\varepsilon_2}{2}\right)\right)\sin(\Delta\phi)$$
$$+(-\xi^2\,\cos(\alpha)\sin(\beta) + \chi^2\,\sin(\alpha)\cos(\beta))\cos\left(\frac{d\varepsilon_1}{2} + \frac{d\varepsilon_2}{2}\right)\cos(\Delta\phi) \tag{6}$$

$$F = \xi\chi\left(\cos(\beta)\,\sin(\beta)\cos\left(\frac{d\varepsilon_1}{2}\right)\,\sin\left(\frac{d\varepsilon_2}{2}\right)\,\sin(2\Delta\phi) + \cos(\alpha)\,\cos(\beta)\,\left(\cos\left(\frac{d\varepsilon_1}{2}\right)\cos\left(\frac{d\varepsilon_2}{2}\right)\right.\right.$$
$$\left. - \sin\left(\frac{d\varepsilon_1}{2}\right)\,\sin\left(\frac{d\varepsilon_2}{2}\right)\,\cos(2\Delta\phi)\right)(+\sin(\alpha)\,\sin(\beta)\left(-\sin\left(\frac{d\varepsilon_1}{2}\right)\,\sin\left(\frac{d\varepsilon_2}{2}\right) + \cos\left(\frac{d\varepsilon_1}{2}\right)\,\cos\left(\frac{d\varepsilon_2}{2}\right)\,\cos(2\Delta\phi)\right)$$
$$\left. + \sin(\alpha)\,\cos(\alpha)\,\sin\left(\frac{d\varepsilon_1}{2}\right)\cos\left(\frac{d\varepsilon_2}{2}\right)\sin(2\Delta\phi)\right) \tag{7}$$

In these equations, $d\varepsilon_1$ and $d\varepsilon_2$ are the ellipticities of the two collinear beams (ideally zero), α and β are the orientation of the two polarizations relative to the polarizing beam splitter axes (together the two ideally zero angles determine both non-orthogonality between the two polarizations and rotation of the polarization axes relative to the polarizing beam splitter), ξ and χ are the transmission coefficients for the polarizing beam splitter (ideally equal to one), and $\Delta\phi = 4\pi n \times \Delta l/\lambda$ is the phase change introduced by a given displacement, Δl (λ is the source wavelength and n is the refractive index for the propagating medium) for a single pass configuration of the interferometer. The displacement error, Δl_{pe}, due to the periodic phase error (Eq. (1)) is given in Eq. (8).

$$\Delta l_{pe} = \frac{\Delta\phi_{pe}\lambda}{4\pi n} \tag{8}$$

An example of the variation in periodic error with nominal displacement is provided in the top panel of Fig. 1. The conditions are: $d\varepsilon_1 = d\varepsilon_2 = 0$, $\alpha = -\beta = 2^\circ$, $\xi = \chi = 1$, $\theta = 20^\circ$, $\lambda = 633$ nm, and $n = 1$. It is seen that first order error dominates. This is highlighted by computing the spatial discrete Fourier transform and normalizing the frequency axis to error order. See the middle panel, where the first and second order error amplitudes are 2.95 nm and 0.15 nm, respectively, for the given conditions. The distribution in error values (lower panel) was determined by Monte Carlo simulation. Because it is equally likely that displacement is recorded at any location along the measurement path in a typical measurement scenario, we described Δl using a uniform distribution with a range from zero to λ and, in each iteration of the Monte Carlo simulation (100,000 total), randomly sampled Δl to determine the nominal phase $\Delta\phi$. This value was then used to compute the periodic error for that iteration using Eqs. (1)–(8). The strongly non-normal distribution seen in the lower panel of Fig. 1 is obtained due to the high slopes around zero values in the nearly sinusoidal error. The standard deviation is 2.09 nm.

A second example is provided in Fig. 2. In this case, both first and second order error are significant for the conditions: $d\varepsilon_1 = d\varepsilon_2 = 0$, $\alpha = -\beta = 20^\circ$, $\xi = \chi = 1$, $\theta = 2^\circ$, $\lambda = 633$ nm, and $n = 1$. Their amplitudes are 2.56 nm and 6.74 nm, respectively. The distribution is again non-normal, but now contains four peaks rather than two due to the second order error contribution. The standard deviation is 5.12 nm. Many other distributions are possible depending on the frequency mixing conditions.

To determine the periodic error uncertainty, we used Monte Carlo simulation. We selected this approach, rather than the first order Taylor series expansion method described in Refs. [35,36], because the periodic error phase in Eq. (1) is identically zero for ideal values of the input variables. Selection of ideal mean values presumes that all misalignments/imperfections have been corrected to within the uncertainty limits (i.e., all known biases have been removed to within the applicable limits).

For demonstration purposes, we chose standard uncertainties of $u(d\varepsilon_1) = 0.1^\circ$, $u(d\varepsilon_2) = 0.1^\circ$, $u(\alpha) = 2^\circ$, and $u(\theta) = 2^\circ$. Normal distributions were assumed in all cases. The corresponding mean values were $d\varepsilon_1 = d\varepsilon_2 = 0^\circ$, $\alpha = \beta = 0^\circ$, and $\theta = 0^\circ$. The transmission coefficients, ξ and χ, are bounded by a maximum value of 1. Therefore, we selected a uniform distribution with a range of ± 0.05 about a mean value of 0.95 for each.[1] Uncertainties in λ and n were not considered at this stage; they are treated in Section 4 where the remaining displacement uncertainty contributors are added. Finally, we used $\lambda = 633$ nm and $n = 1$ and again applied a uniform distribution for Δl with a range from zero to λ. Results are provided in Fig. 3, which shows the distribution of Δl_{pe} values for the selected input uncertainties. The mean value is zero and the standard deviation is 1.77 nm (100,000 iterations). The reader may note that the distribution is non-normal, with a higher likelihood of obtaining zero error than a normal distribution would suggest.

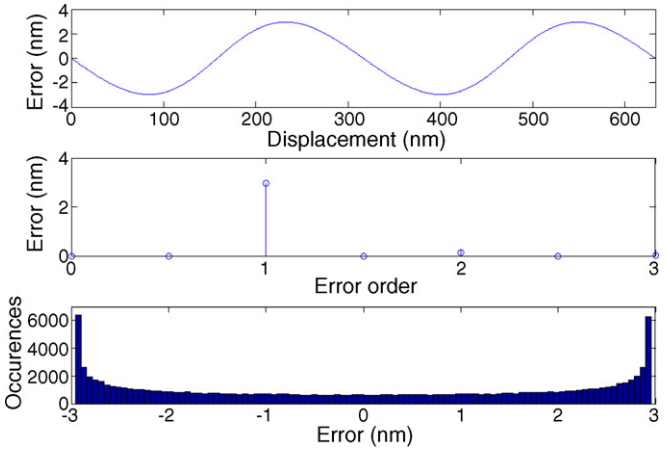

Fig. 1. (Top) periodic error as a function of nominal displacement for $d\varepsilon_1 = d\varepsilon_2 = 0, \alpha = -\beta = 2^\circ, \xi = \chi = 1, \theta = 20^\circ, \lambda = 633$ nm, and $n = 1$; (middle) spatial Fourier transform of periodic error with the frequency axis normalized to error order (i.e., 1 represents first order error); (bottom) distribution of periodic error.

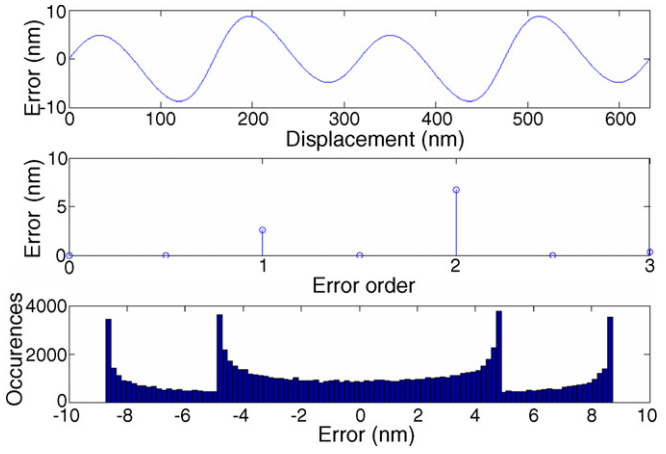

Fig. 2. (Top) periodic error for $d\varepsilon_1 = d\varepsilon_2 = 0$, $\alpha = -\beta = 20^\circ$, $\xi = \chi = 1$, $\theta = 2^\circ$, $\lambda = 633$ nm, and $n = 1$; (middle) spatial Fourier transform of periodic error; (bottom) distribution of periodic error.

As an exercise, the products of the sensitivities, $\partial\Delta l_{pe}/\partial x$, and standard uncertainties, $u(x)$, for each input x were calculated; see Table 1. The individual contributors were isolated by setting all uncertainties except the term in question equal

[1] The standard deviation for this case is $0.05/\sqrt{3}$ [36].

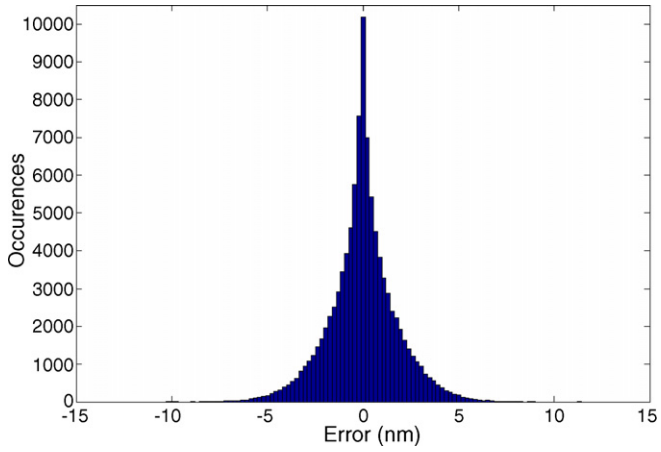

Fig. 3. Histogram of Δl_{pe} values for normal distributions of $d\varepsilon_1$, $d\varepsilon_2$, α, β, and θ with $u(d\varepsilon_1) = u(d\varepsilon_2) = 0.1^\circ$, $u(\alpha) = u(\beta) = u(\theta) = 2^\circ$ and zero mean values; and uniform distributions of ξ and χ with ranges of ± 0.05 and mean values of 0.95.

to zero. Presumably, this would enable the individual contributors to be compared, similar to the error budget and analytical first order Taylor series approaches. However, as seen in the table, the apparent individual contributions for ξ, χ, and θ are zero. This is clearly not the case. Rather, these terms are only zero for ideal mean values and no variation in all other inputs. For any other case, their contributions are non-zero. This emphasizes the utility of using the Monte Carlo technique to simultaneously consider all uncertainties for this evaluation.

3. Periodic error measurements

A photograph and schematic of the experimental setup are provided in Fig. 4. The orthogonal, linearly polarized beams with a split frequency of 3.65 MHz (Helium-Neon laser source) first pass through a half-wave plate. Rotation of the half-wave plate enables variation in the apparent angular alignment (about the beam axis) between the polarization axes and polarizing beam splitter. The light is then incident on a non-polarizing beam splitter (80% transmission) that directs a portion of the beam to a fiber optic pickup after passing through a fixed angle sheet polarizer (oriented at 45°). The pickup is mounted on a two rotational degree-of-freedom flexure which enables efficient coupling of the light into the multi-mode fiber optic. This signal is used as the phase reference in the measurement electronics.

The remainder of the light continues to the polarizing beam splitter where it is separated into its two frequency components that travel separately to the moving and fixed retroreflectors. Motion of the moving retroreflector is achieved using an air bearing stage. After the beams are recombined in the polarizing beam splitter, they are directed by a 90° prism through a polarizer with a variable rotation angle. Finally, the light is launched into a fiber optic pickup. This serves as the measurement signal in the measurement electronics (0.3 nm resolution for the single pass configuration used in this study).

The intent of the setup design was to minimize other error contributors and enable variation in the periodic error nature (i.e., first or second order) and amplitude. To isolate periodic error, the setup was designed with zero dead path difference (i.e., the distance between the polarization beam splitter and the moving retroreflector was equal to the distance between the polarization beam splitter and the fixed retroreflector at initialization) and small Abbe offset (25 mm). The measurement time (~100 ms) and motion amplitude were kept small to minimize the contribution of air refractive index variations due to the environmental changes [17]. Additionally, careful alignment of the air bearing stage axis with the optical axis resulted in small cosine error and beam shear.

Example comparisons between measurement results and the Cosijns et al. model for constant velocity motions are provided in Figs. 5 and 6. In both instances the periodic error content was isolated (for viewing purposes) by performing a least squares linear regression and subtracting the best fit line. For Fig. 5, the polarizer was rotated 39° from its nominal 45° orientation in order to provide a scenario with significant first order error. The other model parameters were: $n = 1$, $\lambda = 633$ nm, $d\varepsilon_1 = d\varepsilon_2 = 0^\circ$, $\alpha = -\beta = 1.5^\circ$, and $\xi = \chi = 1$. In Fig. 6, the half-wave plate was adjusted 10° from its nominal orientation (fast axis vertical). In this case, both first and second order errors were present. The model parameters were: $n = 1$, $\lambda = 633$ nm, $d\varepsilon_1 = d\varepsilon_2 = 0^\circ$, $\alpha = -\beta = 20^\circ$,[2] $\theta = 2^\circ$, and $\xi = \chi = 1$. Good agreement is seen. In both cases, the phase measuring electronics used a sampling frequency of 312.5 kHz.

To evaluate the Monte Carlo approach to periodic error uncertainty evaluation, two sets of measurements were performed. First, the polarizer angle was varied from −41° to +37° about the nominal value and the first and second order errors identified using the Fourier transform approach described in Section 2. Second, the half-wave plate angle was varied from −16° to +14° about its nominal value and the periodic error determined. These measurement results were compared to model predictions using nominal input values: (1) Fig. 7 shows results for the polarizer tests with $n = 1$, $\lambda = 633$ nm, $d\varepsilon_1 = d\varepsilon_2 = 0^\circ$, $\alpha = -\beta = 1.5^\circ$, $\theta = -41^\circ$ to $+37^\circ$, and $\xi = \chi = 1$; (2) Fig. 8 displays the half-wave plate results with $n = 1$, $\lambda = 633$ nm, $d\varepsilon_1 = d\varepsilon_2 = 0^\circ$, $\alpha = -\beta = -32^\circ$ to $+28^\circ$, $\theta = 2^\circ$, and $\xi = \chi = 1$. These figures also

Table 1
Apparent individual uncertainty contributors for Δl_{pe}

x	$\bar{x}$	$u(x)$	$(\partial \Delta l_{pe}/\partial x)u(x)$ (nm)
$d\varepsilon_1$	0	0.1°	0.03
$d\varepsilon_2$	0	0.1°	0.03
α	0	2°	1.25
β	0	2°	1.25
ξ	0.95[a]	$0.05/\sqrt{3}$	0
χ	0.95[a]	$0.05/\sqrt{3}$	0
θ	0	2°	0

[a] The mean value was set equal to 1 when evaluating other inputs.

[2] A 1° rotation of the half wave plate gives a 2° change in the linear polarization angle.

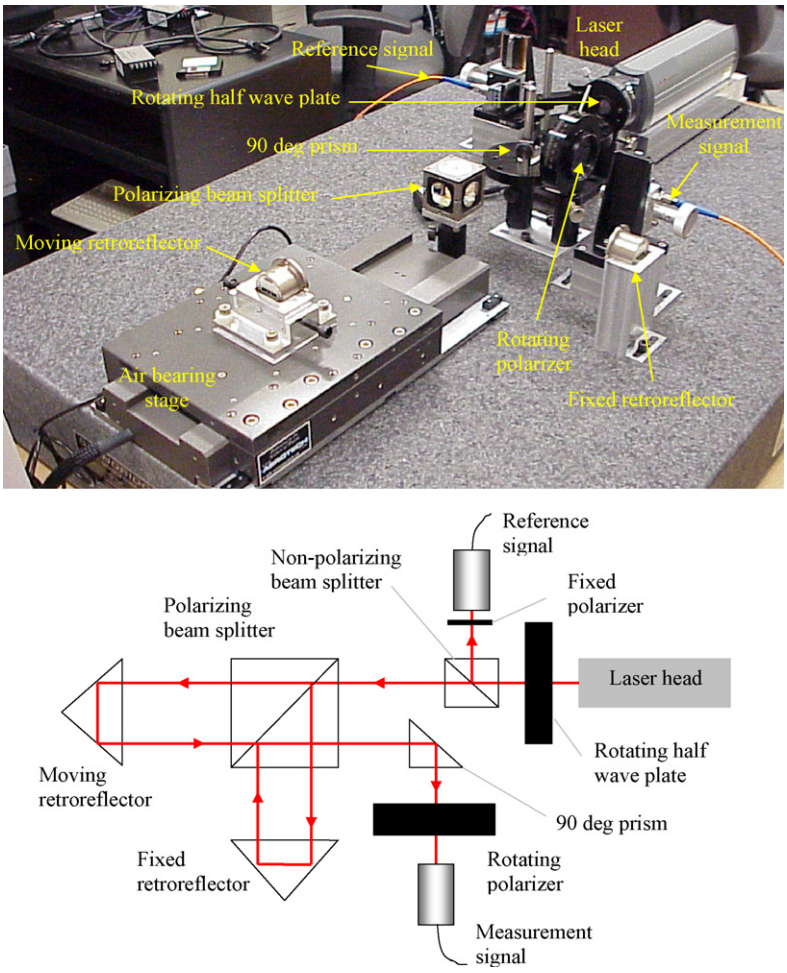

Fig. 4. (Top) photograph of single pass, heterodyne interferometer experimental setup; (bottom) schematic of setup.

show mean values from Monte Carlo simulations, where the Monte Carlo results include one standard deviation (1σ) error bars which reflect the input uncertainties identified in Table 2. In the top panel of Fig. 7, good agreement is seen. Additionally, for polarizer angles near the nominal value (axis value of zero) it is observed that the Monte Carlo means (dotted line) are larger than the model values (squares). This trend matches the experimental results (circles). In the bottom panel, reasonable agreement is observed, but the measured errors lie outside

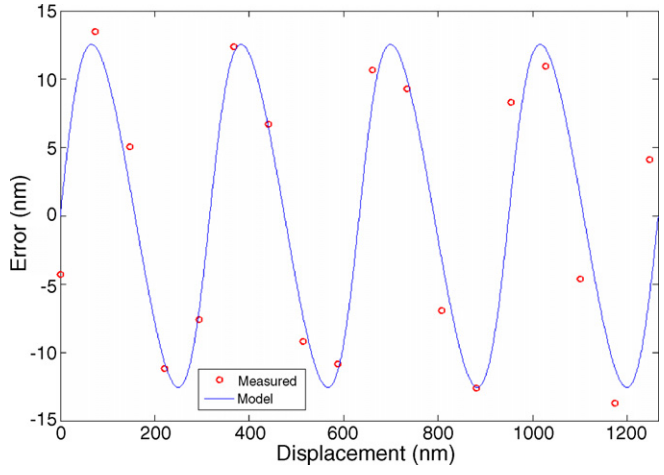

Fig. 5. Measurement/model comparison for 39° polarizer misalignment—first order error dominates. Other model parameters were: $n=1$, $\lambda=633$ nm, $d\varepsilon_1=d\varepsilon_2=0°$, $\alpha=-\beta=1.5°$, and $\xi=\chi=1$.

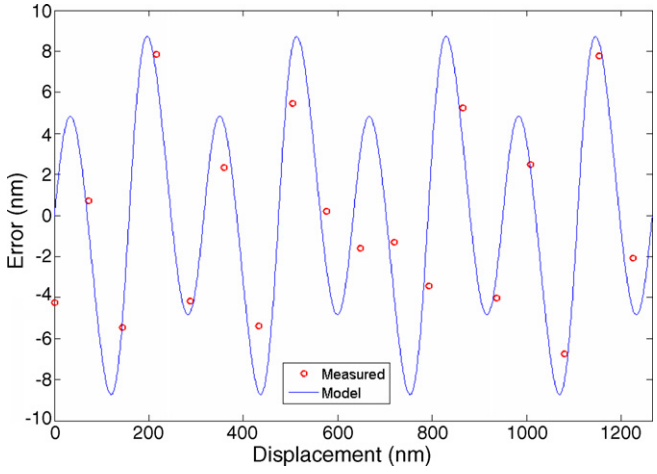

Fig. 6. Measurement/model comparison for 10° half-wave plate misalignment—first and second order errors are present. Model parameters were: $n=1$, $\lambda=633$ nm, $d\varepsilon_1=d\varepsilon_2=0°$, $\alpha=-\beta=20°$, $\theta=2°$, and $\xi=\chi=1$.

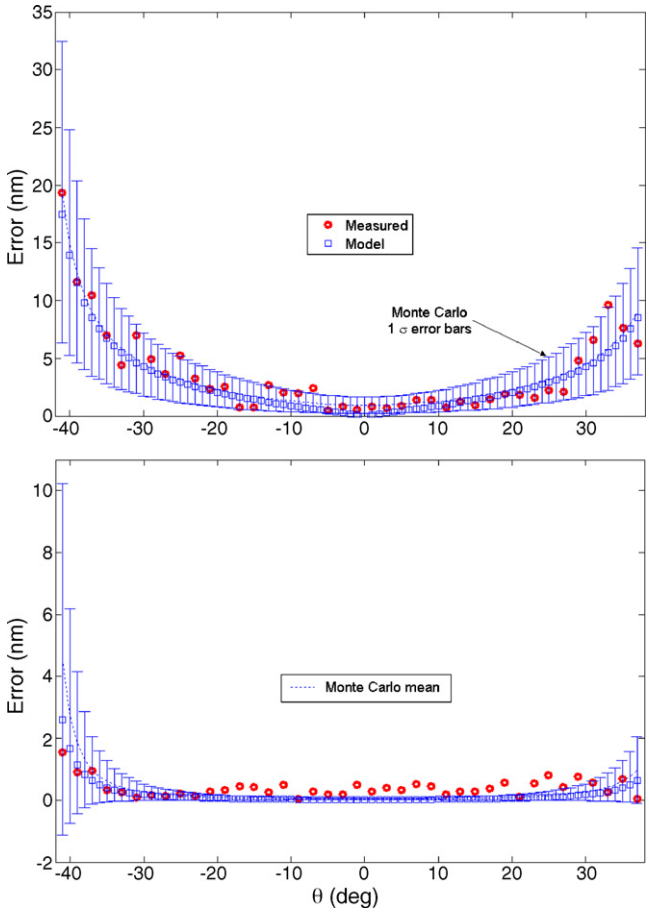

Fig. 7. Comparisons between measurements (circles), model (squares), and Monte Carlo simulation (dotted line) for variable polarizer angle tests. (top) First order errors; (bottom) second order errors.

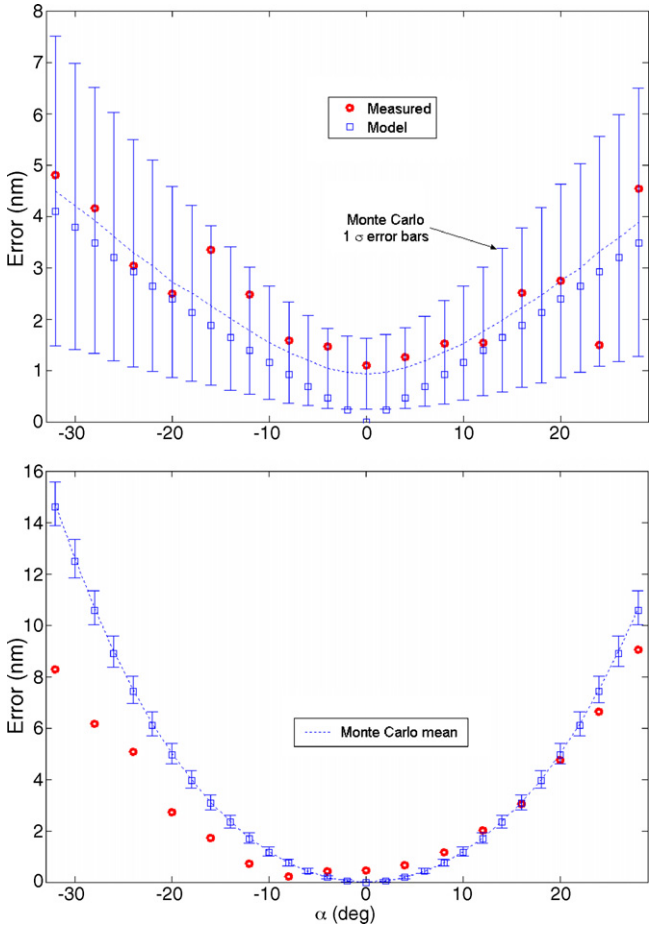

Fig. 8. Comparisons between measurements (circles), model (squares), and Monte Carlo simulation (dotted line) for variable half-wave plate angle tests. (top) First order errors; (bottom) second order errors.

the 1σ error bars for small angles. These error levels approach the resolution limit (0.3 nm), which was not considered as an uncertainty contributor at this stage. In the top panel of Fig. 8, the larger Monte Carlo mean errors near the nominal half-wave plate angle again more closely agree with experiment that the model values determined from mean inputs. In the bottom panel, although the general trends agree, the experimental errors generally fall outside the Monte Carlo error bars. This could be the result of incorrect estimates of the mean input values or limitations of the Fourier-based identification of error levels. In both figures, it can be seen that the first order errors are generally more sensitive to input variations than the second order errors (from the relative sizes of the error bars).

Table 2
Monte Carlo simulation input values for first and second order error uncertainty evaluation (all distributions were normal except for ξ and χ which were uniform)

Polarizer tests			Half-wave plate tests	
X	$\bar{x}$	$u(x)$	$\bar{x}$	$u(x)$
$d\varepsilon_1$	0	0.1°	0	0.1°
$d\varepsilon_2$	0	0.1°	0	0.1°
α	1.5	1°	−32 to +28°	1°
β	−1.5	1°	+32 to −28°	1°
ξ	0.95	$0.05/\sqrt{3}$	0.95	$0.05/\sqrt{3}$
χ	0.95	$0.05/\sqrt{3}$	0.95	$0.05/\sqrt{3}$
θ	−41 to +37°	1°	2	1°

The Monte Carlo simulations for first and second order uncertainty evaluation in Figs. 7 and 8 required the following steps: (1) sample the input values for $d\varepsilon_1$, $d\varepsilon_2$, α, β, θ, ξ, and χ from the predefined distributions (see Table 2); (2) calculate the periodic error profile using the Cosijns et al. model; (3) identify the first and second order periodic error amplitudes using the Fourier transform approach; (4) record the results for each simulation iteration. The mean values and standard deviations from all iterations (10,000) were then taken to represent the best estimates of the first and second order error expectation values and standard uncertainties, respectively.

4. Displacement combined standard uncertainty

In this section, additional displacement uncertainty contributors are described and the analytical displacement equation is provided.

4.1. Abbe error

The potential for Abbe error exists whenever the measurement beam is not collinear with the motion axis. The

relationship between the true, l, and measured, l_m, displacement is $l = l_m - AO\tan(\psi)$, where AO is the Abbe offset between the measurement beam and motion axis and ψ is uncompensated rotation about a line normal to the plane containing both the measurement beam and motion axis.

4.2. Cosine error

Cosine error is inherent to displacement measurement interferometry because the beam and motion axis cannot be perfectly aligned (i.e., some uncertainty always remains). The corresponding true/measured displacement relationship is $l = l_m \sec(\gamma)$, where γ is the (positive or negative) angular misalignment. The reader may note that, for any non-zero value of γ, the measured displacement is always smaller than the true displacement (i.e., a bias is introduced). The reported value, l_r, can be corrected for the bias using $l_r = \bar{l}_m(1 + 0.5u^2(\gamma))$, where $\bar{l}_m$ is the expectation value of l_m and $u^2(\gamma)$ is the variance of γ [35].

4.3. Deadpath error

Deadpath error occurs when the path lengths from the polarizing beam splitter to the reference and measurement targets are unequal at initialization and there is an uncompensated change in the refractive index, Δn, of the propagating medium (we consider air here) during the measurement. The true/measured displacement relationship is $l = l_m - \Delta n \times DP$, where DP is the deadpath, or difference between the path lengths. The value of the refractive index for air may be expressed as a function of absolute temperature, T (K), pressure, P (Pa), percent relative humidity, RH, and carbon dioxide content, CO_2 (ppm) as shown in Eq. (9) [17]. An evaluation of this equation at conditions of standard temperature and pressure (20°C and 101323.2 Pa) with 50% RH and an assumed CO_2 level of 355 ppm yields an air index value of 1.0002713.

$$n = 1 + 271.8 \times 10^{-6}\frac{P}{101325}\frac{293.15}{T} \times \left(1 + 0.54\left(\frac{CO_2 - 300}{1 \times 10^6}\right)\right) - 1 \times 10^{-8}\,RH \quad (9)$$

The reader may note that Eq. (9) does not implicitly consider air turbulence, which affects index through localized time-dependent fluctuations in temperature and pressure [5,39]. This could be incorporated, however, by adding noise (in addition to the variations caused by uncertainties in the temperature, pressure, and relative humidity transducers) to the index values within the Monte Carlo simulation.

4.4. Environmental error

This error occurs when there is an uncompensated change in index during a measurement. The error relationship is $l = l_m - \Delta n \times PD$, where PD is the physical displacement of the moving retroreflector after initialization. Resolution limits in the displacement measurement system can be conveniently included as perturbations in PD.

4.5. Interferometer thermal effects

Changes in temperature, and the associated thermal deformations, can lead to errors associated with the interferometer optics. The corresponding relationship is $l = l_m - \Delta T \times C_{th}$, where ΔT is the change in temperature and C_{th} is a constant typically supplied by the interferometer manufacturer.

4.6. Other phase errors

In addition to periodic error, nonlinearities can also be introduced by the phase measuring electronics, $\Delta\phi_{elect}$ [30,38]. Also, a change in overlap between the reference and measurement beams, or beam shear, during a measurement can lead to errors due to the imperfect, non-planar wavefronts, $\Delta\phi_{shear}$.

4.7. Wavelength stability

Variation in the source wavelength during a measurement naturally leads to errors. The level of variation is small and provided by the laser manufacturer (typically in the form of low to high measurement time intervals).

The final displacement relationship is provided is Eq. (10). This expression considers periodic error as well as the terms identified in Sections 4.1–4.7. To demonstrate the application of Eq. (10), we completed a Monte Carlo simulation to determine $u_c(l)$ for a range of displacements from 1 mm to 1000 mm. The inputs are provided in Table 3 and the simulation results are

Table 3
Monte Carlo simulation input values for $u_c(l)$ evaluation

X	$\bar{x}$	$u(x)$	Distribution type
$d\varepsilon_1$	0	0.1°	Normal
$d\varepsilon_2$	0	0.1°	Normal
α	1°	1°	Normal
β	−2°	1°	Normal
ξ	0.95	$0.05/\sqrt{3}$	Uniform
χ	0.95	$0.05/\sqrt{3}$	Uniform
θ	2	1°	Normal
$\Delta\phi_{elect}$	0	0	–
$\Delta\phi_{shear}$	0	0	–
λ	633 nm	6×10^{-6} nm	Normal
P	101323.2 Pa	$50/\sqrt{3}$ Pa	Uniform
T	20°C	$0.2/\sqrt{3}$ °C	Uniform
RH	50%	$2/\sqrt{3}$%	Uniform
CO_2	355	0	–
AO	0 mm	1 mm	Normal
DP	50 mm	1 mm	Normal
PD	1–1000 mm	$0.3\sqrt{3}$ nm[a]	Uniform
C_{th}	25 nm/°C	1 nm/°C	Normal
γ	0	0.03°	Normal
ψ	100 μrad	10 μrad	Normal

[a] This uncertainty represents the resolution of the interferometer, which depends on the phase measuring electronics and optical configuration.

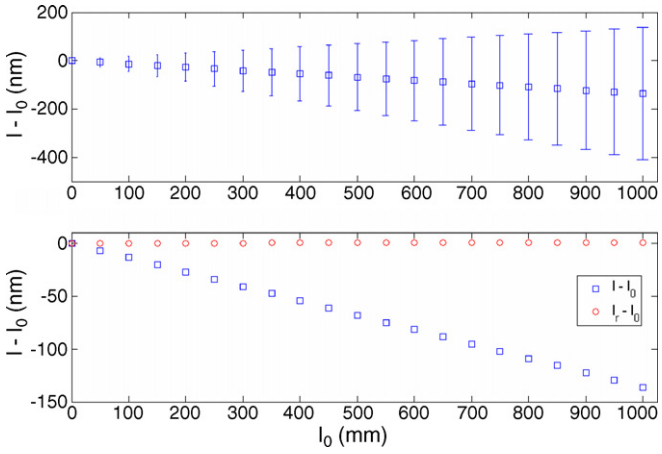

Fig. 9. Monte Carlo simulation results for Eq. (10) using the data in Table 3. (top) Difference between mean Eq. (10) values and nominal displacement with 1σ error bars; (bottom) uncorrected (squares) and corrected (circles) difference.

shown in Fig. 9.

$$l = \frac{(\Delta\phi + \Delta\phi_{\text{pe}} + \Delta\phi_{\text{elect}} + \Delta\phi_{\text{shear}})\lambda}{4\pi n}\cos(\gamma) + \text{AO}\,\tan(\psi) + \Delta n\,\text{DP} + \Delta n\,\text{PD} + \Delta T\,C_{\text{th}} \quad (10)$$

The top panel in Fig. 9 shows both the difference between Eq. (10) mean value and nominal displacement, l_0, and the 1σ error bars (100,000 iterations). As expected, the uncertainty increases substantially over the 1 mm to 1000 mm interval. It is also seen that the mean displacement from Eq. (10) is consistently smaller than the nominal value. This is caused by the single-sided cosine error distribution (note that the bias is present even though the mean value of γ is zero). The bottom panel highlights this bias (squares) and also shows the bias removal using $l_{\text{r}} = \bar{l}_{\text{m}}(1 + 0.5u^2(\gamma))$ (circles).

5. Conclusions

This paper presents a single analytical expression for the displacement recorded using a polarization-coded, heterodyne interferometer in terms of the various uncertainty contributors. These include: (1) phase nonlinearities from non-orthogonality between the ideally linear beam polarizations, elliptical polarization of the individual beams, non-ideal performance of the optical components, and/or mechanical misalignment between the interferometer elements (which combine to give first and second order periodic errors), the phase measuring electronics, and beam shear; (2) Abbe error; (3) cosine error; (4) deadpath error; (5) environmental error; (6) interferometer thermal effects; (7) wavelength stability. The displacement equation is based on the periodic error expression reported by Cosijns et al. Comparisons between this model and experiment for a variety of frequency mixing conditions is provided; good agreement is observed. Monte Carlo simulation is applied to determine the first and second order periodic error bars. The Monte Carlo simulation is then extended to include the other uncertainty contributors included in the analytical displacement equation. A numerical example demonstrates the well-known cosine error bias, as well as the correction of this bias using the variance in the misalignment angle.

Acknowledgements

This work was supported by Agilent Technologies, Inc., the National Science Foundation (DMI-0555645), and Aerotech, Inc. The authors also acknowledge helpful discussions with J. Ziegert, Clemson University.

References

[1] Fedotova G. Analysis of the measurement error of the parameters of mechanical vibrations. Measure Techn 1980;23(7):577–80.
[2] Quenelle R. Nonlinearity in interferometric measurements. Hewlett-Packard J 1983;34(4):10.
[3] Sutton C. Nonlinearity in length measurements using heterodyne laser Michelson interferometry. J Phys E: Sci Instrumen 1987;20:1290–2.
[4] Barash V, Fedotova G. Heterodyne interferometer to measure vibration parameters. Measure Techn 1984;27(7):50–1.
[5] Bobroff N. Residual errors in laser interferometry from air turbulence and nonlinearity. Appl Optics 1987;26(13):2676–82.
[6] Rosenbluth A, Bobroff N. Optical sources of nonlinearity in heterodyne interferometers. Precis Eng 1990;12(1):7–11.
[7] Stone J, Howard L. A simple technique for observing periodic nonlinearities in Michelson interferometers. Precis Eng 1998;22(4):220–32.
[8] Patterson S, Beckwith J. Reduction of systematic errors in heterodyne interferometric displacement measurement. In: Proceedings of the Eighth International Precision Engineering Seminar (IPES). France: Compiegne; 1995. p. 101–4.
[9] Badami V, Patterson S. A frequency domain method for the measurement of nonlinearity in heterodyne interferometry. Precis Eng 2000;24(1):41–9.
[10] Badami V, Patterson S. Investigation of nonlinearity in high-accuracy heterodyne laser interferometry. In: Proceedings of the 12th Annual American Society for Precision Engineering (ASPE) Conference. 1997. p. 153–6.
[11] Wu C, Deslattes R. Analytical modeling of the periodic nonlinearity in heterodyne interferometry. Appl Optics 1998;37(28):6696–700.
[12] Wu C, Su C. Nonlinearity in measurements of length by optical interferometry. Measure Sci Technol 1996;7:62–8.
[13] Hou W, Wilkening G. Investigation and compensation of the nonlinearity of heterodyne interferometers. Precis Eng 1992;14(2):91–8.
[14] Hou W, Zhao X. Drift of nonlinearity in the heterodyne interferometer. Precis Eng 1994;16(1):25–35.
[15] Howard L, Stone J. Computer modeling of heterodyne interferometer errors. Precis Eng 1995;12(1):143–6.
[16] Tanaka M, Yamagami T, Nakayama K. Linear interpolation of periodic error in a heterodyne laser interferometer at subnanometer levels. IEEE Trans Instrument Measure 1989;38(2):552–4.
[17] Bobroff N. Recent advances in displacement measuring interferometry. Measure Sci Technol 1993;4:907–26.
[18] Steinmetz C. Sub-micron position measurement and control on precision machine tools with laser interferometry. Precis Eng 1990;12(1):12–24.
[19] Cretin B, Xie W, Wang S, Hauden D. Heterodyne interferometers: practical limitations and improvements. Optics Commun 1988;65(3):157–62.
[20] Petru F, Cip O. Problems regarding linearity of data of a laser interferometer with a single-frequency laser. Precis Eng 1999;23(1):39–50.
[21] Augustyn W, Davis P. An analysis of polarization mixing errors in distance measuring interferometers. J Vacuum Sci Technol B 1990;8(6):2032–6.
[22] Xie Y, Yu Y. Zeeman laser interferometer errors for high precision measurements. Appl Optics 1992;31(7):881–4.
[23] De Freitas J, Player M. Importance of rotational beam alignment in the generation of second harmonic errors in laser heterodyne interferometry. Measure Sci Technol 1993;4:1173–6.

[24] De Freitas J, Player M. Polarization effects in heterodyne interferometry. J Modern Optics 1995;42(9):1875–99.
[25] De Freitas J. Analysis of laser source birefringence and dichroism on nonlinearity in heterodyne interferometry. Measure Sci Technol 1997;8:1356–9.
[26] Li B, Liang J. Effects of polarization mixing on the dual-wavelength heterodyne interferometer. Appl Optics 1997;36(16):3668–72.
[27] Park B, Eom T, Chung M. Polarization properties of cube-corner retroreflectors and their effects on signal strength and nonlinearity in heterodyne interferometers. Appl Optics 1996;35(22):4372–80.
[28] Wu C, Lawall J, Deslattes R. Heterodyne interferometer with subatomic periodic nonlinearity. Appl Optics 1999;38(19):4089–94.
[29] Oldham N, Kramar J, Hetrick P, Teague E. Electronic limitations in phase meters for heterodyne interferometry. Precis Eng 1993;15(3):173–9.
[30] Schmitz T, Beckwith J. An investigation of two unexplored periodic error sources in differential-path interferometry. Precis Eng 2002;27(3):311–22.
[31] Chu D, Ray A. Nonlinearity measurement and correction of metrology data from an interferometer system. In: Proceedings of Fourth Euspen International Conference. Scotland (UK): Glasgow; 2004. p. 300–1.
[32] Donaldson R. Error budgets. In: Hocken R, editor. Technology of machine tools. Machine tool accuracy, vol. 5. Machine Tool Task Force (UCRL-52960-5); 1980.
[33] Slocum A. Precision machine design. Englewood Cliffs, NJ: Prentice Hall; 1992.
[34] Schmitz T, Evans C, Davies A, Estler WT. Displacement uncertainty in interferometric radius measurements. Ann CIRP 2002;51(1):451–4.
[35] International Organization for Standardization (ISO). Guide to the Expression of Uncertainty in Measurement. Geneva 1995.
[36] Taylor B, Kuyatt C. NIST Technical Note 1297 Guidelines for Evaluating and Expressing the Uncertainty of NIST Measurement Results. Gaithersburg, MD 1994.
[37] Cosijns S, Haitjema H, Schellekens P. Modeling and verifying non-linearities in heterodyne displacement interferometry. Precis Eng 2002;26:448–55.
[38] Oldham N, Kramar J, Hetrick P, Teague E. Electronic limitations in phase meters for heterodyne interferometry. Precis Eng 1993;15(3):173–9.
[39] Estler WT. High-accuracy displacement interferometry in air. Appl Optics 1985;24:808–15.